

FOURIER-PADÉ APPROXIMATIONS AND FILTERING FOR THE SPECTRAL SIMULATIONS OF INCOMPRESSIBLE BOUSSINESQ CONVECTION PROBLEM *

M. S. MIN, S. M. KABER, W. S. DON, †

Abstract. In this paper, we present the rational approximations based on Fourier series representation. Considering periodic piecewise analytic functions, the well known Gibbs phenomenon deteriorates the convergence of the standard Fourier method. Here, for a given set of the Fourier coefficients from a periodic piecewise analytic function, we define Fourier-Padé-Galerkin and Fourier-Padé collocation methods by expressing the coefficients for the rational approximations using the Fourier data. It is shown that those methods converge exponentially in the smooth region and successfully reduce the Gibbs oscillations as the degrees of the denominators and the numerators of Padé approximants increase.

Numerical results are demonstrated for several examples and the collocation method is applied as a post-processing to the standard pseudospectral simulations for the one dimensional inviscid Burgers' equation and the two dimensional incompressible inviscid Boussinesq convection flow.

Key words. Rational approximation, Gibbs phenomenon, Fourier-Padé Galerkin, Fourier-Padé collocation, post-processing

AMS subject classifications. 41A20, 41A21, 41A25, 65T10, 65T20

1. Introduction. In this paper, we discuss a rapidly converging approximation to finite Fourier series, by defining a rational function which denominator and numerator are represented in finite Fourier sum. The underlying principle of rational approximation was proposed by H. Padé in 1892 [4, 13]. Since then, with the advent of computer in 1950's, Padé rational approximations have been studied as one of the popular computational methods of representing functions, especially rapidly converging functions. They are generally more efficient than polynomial approximations with a reduced number of operations for the same accuracy [5, 6, 7, 8, 16].

The main objective in this paper is to present simple computing algorithms for Fourier-Padé rational approximation for discontinuous functions and its application as a filter to accelerate the convergence of the oscillatory pseudospectral solutions of nonlinear partial differential equations, in particular inviscid Burgers' equation and incompressible Boussinesq convection flow in the absence of viscosity.

Fourier methods are powerful numerical tools for approximating periodic analytic functions with spectral convergence. However considering periodic piecewise analytic functions, the well known difficulty of the Fourier methods is the slow rate of convergence $O(\frac{1}{N})$ globally and the oscillations of $O(1)$ near singularity, which is called the Gibbs phenomenon [9, 10, 11].

In order to overcome the oscillatory behaviors of the Fourier methods for discontinuous problems, many numerical techniques have been developed. For a given finite set of Fourier data, the Gegenbauer reconstruction techniques [12] remove the oscillations completely with spectral convergence up to the discontinuity as the degrees of Gegenbauer polynomial expansion increase, when a reasonably accurate information

* This research is supported by Grant DOE-DE.FG02.98ER25346.

† Division of Applied Mathematics, Brown University, Providence, USA, (msmin@cfm.brown.edu, wsdon@cfm.brown.edu)

Laboratoire Jacques-Louis Lions Université Paris VI, France, (kaber@ann.jussieu.fr). This work was done while this author was visiting the Division of Applied Mathematics, Brown University, Providence, USA.

for the location of discontinuities is provided.

However with no knowledge of the singularity, Padé reconstruction recovers back a non-oscillatory solution successfully with a reduced overshoot at the singularity. It is due to the fact that the possible existence of poles of some order for the denominator of Padé approximant allows to give a better approximation to the functions exhibiting singular behaviors such as large gradient and discontinuity.

In [8], it is shown a way of implementing the rational trigonometric approximations for even or odd 2π -periodic piecewise smooth functions and the application to the solution of an initial boundary value problem for a simple heat equation. In his work, Fourier-Padé approximants are defined in a nonlinear way such that the relation between the coefficients of the rational approximations and the Fourier coefficients involves a necessary procedure of calculating the integration of rational functions, which makes the numerical scheme relatively complicated. And the study for the general case rather than even or odd function is not presented. In [7], Fourier expansion is treated as a Laurent expansion, and using Fourier-Padé rational approach the spectral convergence is obtained up to the discontinuity by subtracting off the jump from the Fourier data, which requires the advance knowledge of the singularity.

Here we present two Fourier-Padé methods considering the general case of piecewise analytic functions with no advance knowledge of the singularity. Simple ways of implementing Fourier-Padé Galerkin and Fourier-Padé collocation methods are demonstrated and applied to simulate the solutions of nonlinear partial differential equations. For the hyperbolic partial differential equations such as Burgers' equation, an initially smooth function can evolve into shock in time for inviscid case and large gradient for viscous case. Therefore the standard spectral simulations will exhibit the Gibbs phenomenon and deteriorate the accuracy of the numerical solutions in time. From accurate Fourier data computed by Fourier method, we apply the Fourier-Padé reconstruction as a post-processing. After the post-processing, the computational results show successful reduction of the non-physical oscillations in the standard spectral solutions of the one dimensional inviscid Burgers' equation and the two dimensional inviscid Boussinesq equations. Further study has to be established to find the optimal relation between the degrees of the polynomial of the Padé approximants and the number of the Fourier coefficients.

This paper is organized as follows. In section 2, Fourier-Padé-Galerkin method is discussed. The Fourier-Padé-Galerkin coefficients of the denominator are explicitly represented as a linear combination of the given Fourier coefficients. The numerical computations by this method are carried out by the sawtooth function.

Section 3 introduces a new method using collocation points which will be favorably used in applications. The explicit formulations for the Fourier-Padé collocation coefficients are presented in a similar manner as the case for Fourier-Padé Galerkin method. The sawtooth function is again considered for numerical simulations.

Section 4 demonstrates the successful improvement of Fourier-Padé collocation methods in mitigating the oscillations near the sharp gradient for the spectral solutions of the one dimensional inviscid Burgers' equation and two dimensional incompressible inviscid Boussinesq convection flow. Section 5 concludes.

2. Fourier-Padé Galerkin Approximation. Let \mathcal{S}_N be the space of trigonometric polynomials of degree N defined as

$$(2.1) \quad \mathcal{S}_N = \text{span}\{e^{inx} \mid -N \leq n \leq N\}.$$

Consider a piecewise analytic 2π -periodic function $u(x)$ in $[-\pi, \pi]$. We define the Fourier-Padé Galerkin approximation of u by

$$(2.2) \quad R_{K,M} = \frac{P_K}{Q_M},$$

where $P_K \in \mathcal{S}_K$ and $Q_M \in \mathcal{S}_M$, such that

$$(2.3) \quad (Q_M u - P_K, v) = 0 \text{ for all } v \in \mathcal{S}_{K+M},$$

with the inner product defined by

$$(2.4) \quad (u, v) = \frac{1}{2\pi} \int_{-\pi}^{\pi} u(x) \overline{v(x)} dx.$$

Let us denote

$$(2.5) \quad P_K = \sum_{k=-K}^K b_k e^{ikx} \text{ and } Q_M = \sum_{m=-M}^M c_m e^{imx}.$$

The Fourier series representation of u is expressed by

$$(2.6) \quad u(x) = \sum_{n=-\infty}^{\infty} \hat{u}_n e^{inx},$$

where

$$(2.7) \quad \hat{u}_n = \frac{1}{2\pi} \int_{-\pi}^{\pi} u(x) e^{-inx} dx.$$

Then, substitute P_K , Q_M and $v = e^{inx}$ for $-(K+M) \leq n \leq K+M$ to (2.3), one obtains the following equations:

$$(2.8) \quad b_k = \sum_{m=-M}^M c_m \hat{u}_{k-m} \quad \text{for } |k| \leq K,$$

and

$$(2.9) \quad \sum_{m=-M}^M c_m \hat{u}_{n-m} = 0 \quad \text{for } K < |n| \leq K+M.$$

The system of the equations (2.9) can be written in a matrix form, $\mathbf{A}\mathbf{c} = 0$, where $\mathbf{c} = [c_M, \dots, c_{-M}]^T$ and $2M \times (2M+1)$ matrix \mathbf{A} defined by

$$(2.10) \quad \mathbf{A} = \begin{bmatrix} \hat{u}_{-K-2M} & \dots & \hat{u}_{-K-M} & \dots & \hat{u}_{-K} \\ \hat{u}_{-K-2M+1} & \dots & \hat{u}_{-K-M+1} & \dots & \hat{u}_{-K+1} \\ \vdots & & & & \vdots \\ \hat{u}_{-K-M-1} & \dots & \hat{u}_{-K-1} & \dots & \hat{u}_{-K+M-1} \\ \hat{u}_{-K-M+1} & \dots & \hat{u}_{K+1} & \dots & \hat{u}_{K+M+1} \\ \vdots & & & & \vdots \\ \hat{u}_{K-1} & \dots & \hat{u}_{K+M-1} & \dots & \hat{u}_{K+2M-1} \\ \hat{u}_K & \dots & \hat{u}_{K+M} & \dots & \hat{u}_{K+2M} \end{bmatrix}.$$

We solve this linear system numerically using MATLAB subroutine Null(A) which gives the basis of the kernel of the $2M \times (2M + 1)$ matrix A . Once one obtains a set of the coefficients $\{c_m\}_{m=-M}^M$, the coefficients $\{b_k\}_{k=-K}^K$ can be computed from the equation (2.8).

Note that the continuous Fourier coefficients involved in computing b_k 's and c_m 's are

$$(2.11) \quad \{\hat{u}_n\}_{n=-(K+2M)}^{K+2M},$$

and the notation N will denote $N = K + 2M$.

Example 1. We demonstrate the numerical results of the Fourier-Padé Galerkin approximation for a sawtooth function

$$(2.12) \quad u(x) = \begin{cases} x + \pi & \text{for } x \in [-\pi, 0), \\ x - \pi & \text{for } x \in [0, \pi], \end{cases}$$

for which the continuous Fourier coefficients are $\hat{u}_0 = 0$ and $\hat{u}_n = -i/n$ for $n = \pm 1, \pm 2, \dots$.

The left figure in FIG. 2.1 illustrates the Gibbs phenomenon when the standard Fourier Galerkin approximation is applied to the sawtooth function for the number of Fourier modes $N = 8, 16, 32$. The right figure in FIG. 2.1 shows the reconstructed sawtooth function using the Fourier-Padé-Galerkin approximant (solid line). The Gibbs oscillation is clearly being reduced near the discontinuity.

The pointwise errors are shown in FIG. 2.2. In the left figure, for a given fixed $N = 32$, the degree M of the denominator of the Padé approximant is increased. For $M = 0$, it is exactly the standard Fourier-Galerkin method and the pointwise errors only decay like $O(\frac{1}{N})$ away from the discontinuity and the $O(1)$ accuracy is observed clearly at the location of the jump. By increasing the degree M of the denominator, the errors decay exponentially away from the discontinuity as M increases. For a fixed $M = 2$, the rate of convergence of the pointwise error away from the discontinuity is only linear as N increases.

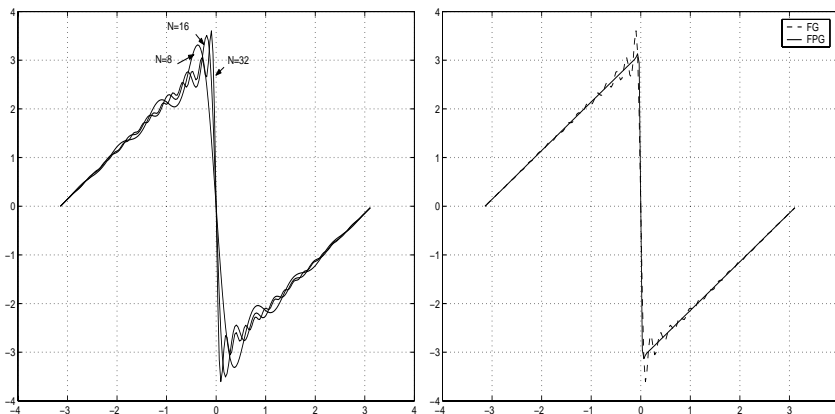


FIG. 2.1. The Gibbs oscillations by Fourier-Galerkin (FG) approximation (left) and Fourier-Padé-Galerkin (FPG) reconstruction (right) for the sawtooth function.

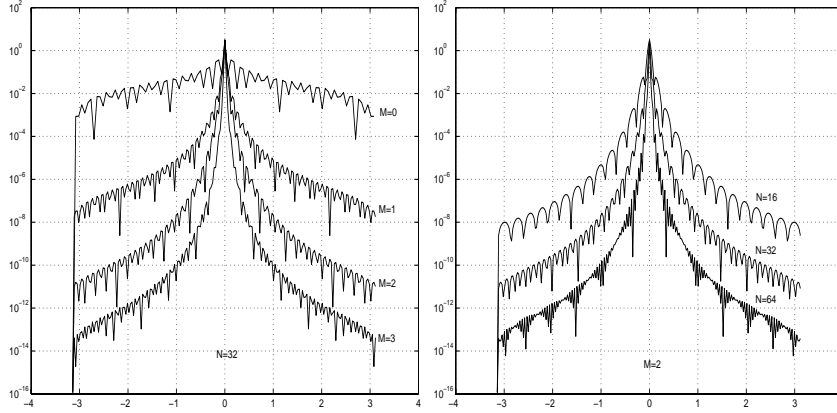


FIG. 2.2. The convergence of the pointwise errors after the Fourier-Padé-Galerkin reconstruction for the sawtooth function with a fixed N (left) and a fixed M (right), respectively.

3. Fourier-Padé Collocation Approximation. Let \mathcal{I}_N be the space of the trigonometric polynomial of degree N , defined as

$$(3.1) \quad \mathcal{I}_N = \text{span}\{e^{inx} \mid -N \leq n \leq N-1\}.$$

Consider a set of even number of grid points

$$(3.2) \quad x_j = -\pi + \frac{\pi j}{N} \quad j = 0, \dots, 2N-1.$$

We define the Fourier-Padé collocation approximation of u by $R_{K,M}^c = \frac{P_K^c}{Q_M^c}$, where $P_K^c \in \mathcal{I}_K$ and $Q_M^c \in \mathcal{I}_M$ ($K+2M=N$), such that

$$(3.3) \quad (Q_M^c u - P_K^c, v)_N = 0 \text{ for all } v \in \mathcal{I}_{K+M},$$

where the discrete inner product is defined by

$$(3.4) \quad (u, v)_N = \frac{1}{2N} \sum_{j=0}^{2N-1} u(x_j) \overline{v(x_j)}.$$

Denote

$$(3.5) \quad P_K^c = \sum_{k=-K}^{K-1} \tilde{b}_k e^{ikx} \quad \text{and} \quad Q_M^c = \sum_{m=-M}^M \tilde{c}_m e^{imx}.$$

Then, substituting P_K^c , Q_M^c and $v = e^{inx}$ for $-K-2M \leq n \leq K-1+2M$ to (3.3), one obtains the following equations: for $-K \leq k \leq K-1$,

$$(3.6) \quad \tilde{b}_k = \sum_{m=-M}^M \tilde{c}_m \tilde{u}_{k-m},$$

and, for $-K-M \leq n < -K$ and $K-1 < n \leq K-1+M$,

$$(3.7) \quad \sum_{m=-M}^M \tilde{c}_m \tilde{u}_{n-m} = 0,$$

where

$$(3.8) \quad \tilde{u}_n = \frac{1}{2N} \sum_{j=0}^{2N-1} u(x_j) e^{-inx_j}.$$

Following the similar procedure as in section 2, we have a linear system $\tilde{A}\tilde{\mathbf{c}} = 0$ to solve $\tilde{\mathbf{c}}$, where $\tilde{\mathbf{c}} = [\tilde{c}_M, \dots, \tilde{c}_{-M}]^T$ and

$$(3.9) \quad \tilde{A} = \begin{bmatrix} \tilde{u}_{-K-2M} & \cdots & \tilde{u}_{-K-M} & \cdots & \tilde{u}_{-K} \\ \tilde{u}_{-K-2M+1} & \cdots & \tilde{u}_{-K-M+1} & \cdots & \tilde{u}_{-K+1} \\ \vdots & & & & \vdots \\ \tilde{u}_{-K-M-1} & \cdots & \tilde{u}_{-K-1} & \cdots & \tilde{u}_{-K+M-1} \\ \tilde{u}_{K-M+1} & \cdots & \tilde{u}_{K+1} & \cdots & \tilde{u}_{K+M+1} \\ \vdots & & & & \vdots \\ \tilde{u}_{K-1} & \cdots & \tilde{u}_{K+M-1} & \cdots & \tilde{u}_{K+2M-1} \end{bmatrix}.$$

We solve this linear system numerically using MATLAB subroutine Null(\tilde{A}) which gives the basis of the kernel of the $2M \times (2M+1)$ matrix \tilde{A} . Once one obtains a set of the coefficients $\{\tilde{c}_m\}_{m=-M}^M$, the coefficients $\{\tilde{b}_k\}_{k=-K}^{K-1}$ can be computed from the equation (3.6).

Note that the discrete Fourier coefficients involved in computing \tilde{b}_k 's and \tilde{c}_m 's are

$$(3.10) \quad \{\tilde{u}_n\}_{n=-(K+2M)}^{K+2M-1}.$$

Remark 3.1 : The Fourier-Padé collocation approach does not interpolate the function $u(x)$ at the collocation points $x_j = -\pi + \frac{\pi j}{N}$. Since from (3.6) we have

$$\begin{aligned} \tilde{b}_k &= \sum_{m=-M}^M \tilde{c}_m \left(\frac{1}{2N} \sum_{j=0}^{2N-1} u(x_j) e^{-i(k-m)x_j} \right) \\ &= \frac{1}{2N} \sum_{j=0}^{2N-1} u(x_j) Q_M^c(x_j) e^{-ikx_j}, \end{aligned}$$

then

$$P_K^c(x) = \sum_{j=0}^{2N-1} u(x_j) Q_M^c(x_j) \left(\frac{1}{2N} \sum_{k=-K}^{K-1} e^{ik(x-x_j)} \right).$$

Thus we can simplify the Fourier-Padé collocation expansion as follows:

$$(3.11) \quad R_{K,M}^c(x) = \sum_{j=0}^{2N-1} u(x_j) w_j(x),$$

where

$$(3.12) \quad w_j(x) = \frac{Q_M^c(x_j)}{Q_M^c(x)} \left(\frac{1}{2N} \sum_{k=-K}^{K-1} e^{ik(x-x_j)} \right).$$

It is clear that since $K = N - 2M$,

$$w_j(x_i) = \begin{cases} \frac{(N-2M)}{N} & \text{for } x_i = x_j, \\ \text{not always zero} & \text{for } x_i \neq x_j. \end{cases}$$

Thus $w_j(x)$ is not a Lagrange interpolation polynomial with the grids x_j ($0 \leq j \leq 2N - 1$) defined here.

Example 2.

We present the numerical results of the Fourier-Padé collocation method applied to the same example as defined in (2.12). As expected, the behavior of the Fourier-Padé collocation approach is very similar to the one of Fourier-Padé Galerkin approach as shown in the FIG. 3.1 and 3.2.

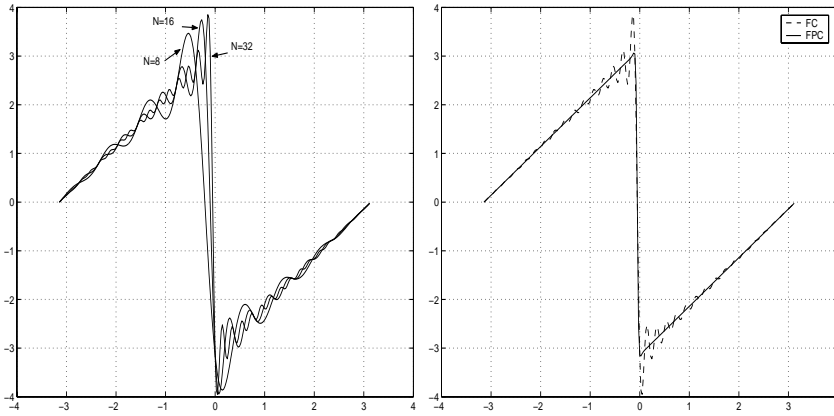


FIG. 3.1. The Gibbs oscillations by Fourier collocation(FC) approximation(left) and Fourier-Padé collocation(FPC) reconstruction(right) for the sawtooth function.

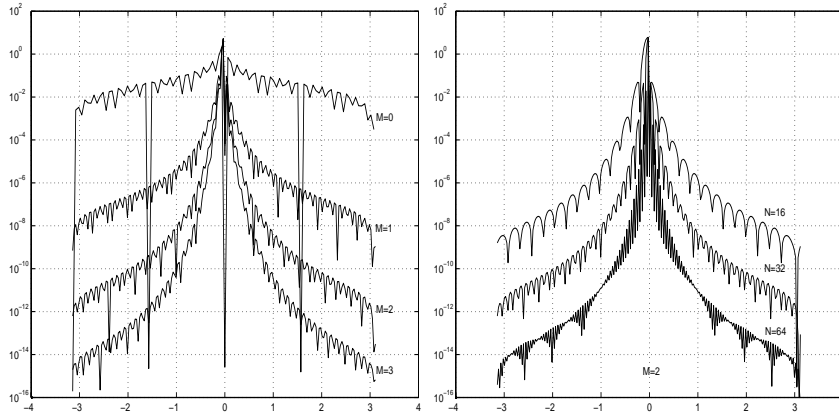


FIG. 3.2. The convergence of the pointwise errors after the Fourier-Padé collocation reconstruction for the sawtooth function with a fixed N (left) and a fixed M (right), respectively.

4. Applications. In this section, we apply the Fourier-Padé-collocation post-processing procedure to the nonlinear hyperbolic and elliptic partial differential equa-

tions for which an initially smooth solution will develop a shock and sharp gradient in time, respectively. The numerical study for the inviscid Burgers' equation and two dimensional incompressible inviscid Boussinesq convection flow is discussed. The algorithm for solving these two problems with periodical boundary condition is straightforward and presented in the literature. The detailed description on the basic building blocks of the algorithm is provided in each subsections.

4.1. Burgers' equation. Burgers' equation is a suitable model for testing computational algorithms for flows where steep gradients or shocks are anticipated since it allows exact solutions for many combinations of initial and boundary conditions. Here we consider inviscid Burgers' equation in one dimension

$$(4.1) \quad \frac{\partial u}{\partial t} + \frac{1}{2} \frac{\partial u^2}{\partial x} = 0,$$

with the initial condition:

$$u(x, 0) = \sin(x).$$

FIG. 4.1 shows the evolution of the exact solution for the Burgers' equation. With the sine wave as an initial condition, the solution forms a stationary shock due to the nonlinearity in (4.1). The numerical solutions performed by the standard Fourier collocation methods are shown in FIG. 4.1(right). The third order Runge-Kutta method is used for time integration and the high frequency components are smoothed out at each time step by using the exponential filter of order 16 in order to stabilize the scheme[18]. As predicted, one can observe the Gibbs oscillations near the shock at $t = 1.5$, which is a natural consequence when one considers the Fourier method to approximate a discontinuous solution.

It is important to note that one should not attempt to reconstruct the function using all the modes in the Fourier spectrum. Depending on the order of the filtering used for the stability of the numerical scheme, only the Fourier coefficients from the lower 1/2 to 2/3 Fourier spectrum are used in the post-processing reconstruction step since the upper portion of the Fourier spectrum doesn't contain high accurate information. Thus the additional parameter for the cut-off frequency N_c should be specified to determine the upper bound of the Fourier mode which information will not contribute in the reconstruction step.

The numerical results in FIG. 4.2 shows the oscillations have been mitigated after the Fourier-Padé reconstruction for the filtered Fourier numerical solutions at $t = 1.5$. The pointwise errors shown in FIG.4.3 demonstrate the successful reduction of the spurious oscillations away from the discontinuity after the Fourier-Padé postprocessing. The exponential decays in errors are observed as N and M increase. Here we use the cut-off frequency $N_c = \frac{N}{2}$.

4.2. Boussinesq equations. In this section, we present some preliminary results on the use of the Fourier-Padé reconstruction to recover the essentially non-oscillatory solution applied to the standard Fourier spectral simulations for the two dimensional incompressible Boussinesq convection flow.

The mass-conservation and the motion for an incompressible inviscid fluid with the gravity as the only body force acting on the fluid in the upward vertical direction has the form

$$(4.2) \quad \frac{\partial \rho}{\partial t} + \mathbf{u} \cdot \nabla \rho = 0,$$

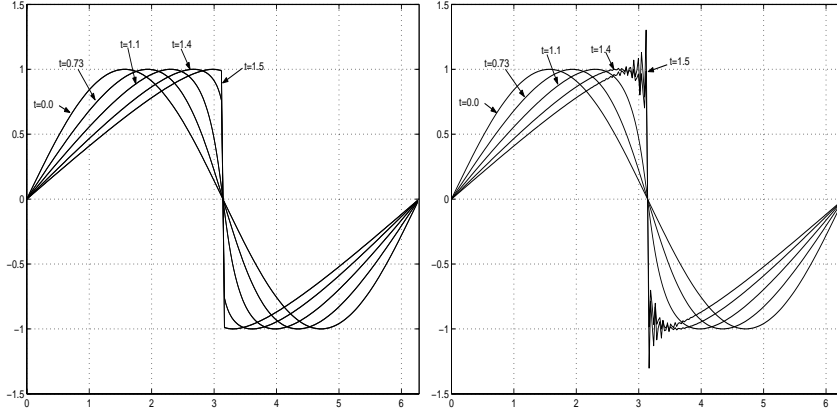


FIG. 4.1. Evolutions of the exact solution(left) and the filtered(order=16) Fourier numerical solutions for inviscid Burgers' equation at different times on grids 256.

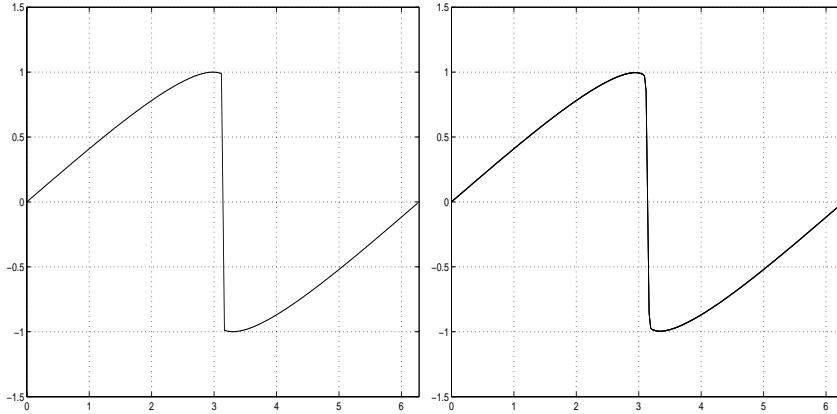


FIG. 4.2. The exact solution(left) and after the Fourier-Padé reconstruction(right) for the filtered Fourier numerical solutions at $t=1.5$. $N_c = 64$ on grids 256.

$$(4.3) \quad \frac{\partial \mathbf{u}}{\partial t} + \mathbf{u} \cdot \nabla \mathbf{u} + \nabla p = \begin{pmatrix} 0 \\ \rho g \end{pmatrix},$$

$$(4.4) \quad \nabla \cdot \mathbf{u} = 0,$$

where ρ is the density(or temperature), $\mathbf{u} = (u, v)$ is the velocity vector, p is the pressure and g is the gravitational constant(normalized to 1).

Now for two-dimensional flow of incompressible fluid in the x - y plane, it satisfies the mass-conservation by writing

$$(4.5) \quad u = \frac{\partial \psi}{\partial y}, \quad v = -\frac{\partial \psi}{\partial x},$$

where the scalar function $\psi(x, y, t)$ is the stream function. Let ω be the vorticity defined by $\omega = \nabla \times \mathbf{u}$. Then the above system can be rewritten as in the following, called stream function-vorticity formulation,

$$(4.6) \quad \frac{\partial \rho}{\partial t} + \mathbf{u} \cdot \nabla \rho = 0,$$

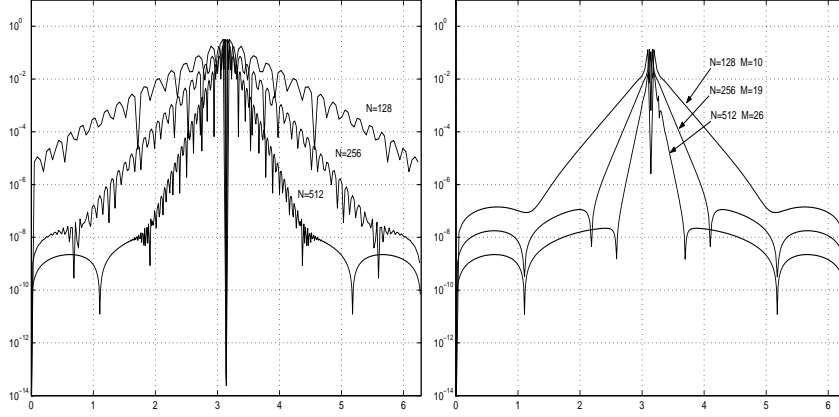


FIG. 4.3. Convergence of the pointwise errors for filtered (order=16) Fourier collocation methods (left) and after the reconstruction by the Fourier-Padé collocation method for the inviscid Burgers' equation at $t = 1.5$

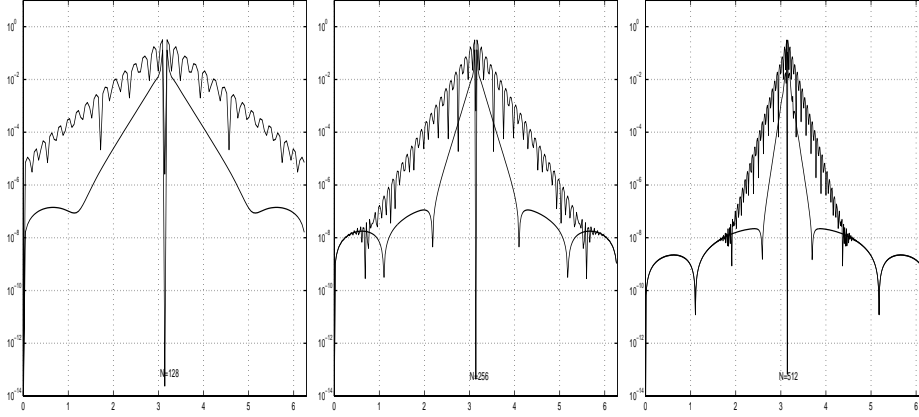


FIG. 4.4. Comparison of the pointwise errors for filtered (order=16) Fourier methods and Fourier-Padé reconstruction for inviscid Burgers' equation at $t = 1.5$ on different size of the grids 128, 256, 512 and $m = 10, 19, 26$, respectively.

$$(4.7) \quad \frac{\partial \omega}{\partial t} + \mathbf{u} \cdot \nabla \omega = -\frac{\partial \rho}{\partial x},$$

$$(4.8) \quad -\Delta \psi = \omega.$$

The initial condition is taken same as the one in [15], consisting of a smooth bubble density in a zero flow field. The density function as an initial data is given as

$$(4.9) \quad \rho(x, y, 0) = 50\rho_1\rho_2(1 - \rho_1),$$

where

$$\rho_1 = \begin{cases} \exp\left(1 - \frac{\pi^2}{\pi^2 - R_1^2}\right) & R_1^2 = x^2 + (y - \pi)^2 < \pi^2, \\ 0 & \text{otherwise,} \end{cases}$$

and

$$\rho_2 = \begin{cases} \exp\left(1 - \frac{R_3^2}{R_3^2 - R_2^2}\right) & R_2 = |x - 2\pi| < R_3 = 1.95\pi, \\ 0 & \text{otherwise.} \end{cases}$$

The density contour at $t = 0$ is shown in FIG. 4.5, computed using on 512^2 grids. For this smooth initial data, the solution remains smooth for a short time as shown in FIG. 4.7. As the bubble rises to the right, the front of the bubble steepens up into a sharp gradient. Large amount of vorticity are generated from the source term in the vorticity equation and deposited around the sharp density edge. Following [3] and [15], one can claim that if a solution develops a singularity in a finite time, then the density gradient should grow exponentially. To resolve the singularity, one would have to refine the grid continuously around the gradient front which is not realistic and practical. Hence, it remains to be a controversial subject of whether there exists a finite time singularity in such flows.

Various computational techniques such as ENO, AMR methods shown in [14], [15], [17], have been developed for simulating the evolution of the bubble with the same initial setup we present here. Their numerical results are consistent with the experimental results in [1] demonstrating the severe deformation of the bubble in the lower part whereas remaining the shape of the bubble on the top.

In this work, the standard Fourier collocation method is used in space considering a periodic boundary condition. The third order TVD Runge-Kutta scheme is used for the evolution in time for the equations of mass-conservation and vorticity production. The exponential filters are applied at each time step in order to maintain the stability of the scheme following a robust way of adding the filters as shown in [18]. The order of filter varies from 12 to 16 as the resolution of the simulation increases. Fourier collocation method used to give disastrous oscillations when the solution develops a large gradient and the number of Fourier modes are not sufficient enough to fully resolve the gradient. Here we investigate a way of suppressing the spurious oscillations near almost singularity and an accurate recovery of the underlying non-oscillatory solution by using Fourier-Padé reconstruction as a post-processing at the final time step. Same as the case for Burgers' equation, it is possible since the Fourier spectral simulation contains accurate information of the solution with high order accuracy.

The Poisson equation (4.8) in the spectral discretization is expressed by $A\psi + \psi B = \omega$ in a matrix equation. To solve this linear system to compute a vector ψ on the discretization for a given vorticity ω , the matrices A and B are casted in the lower and upper Schur form and the transformed system is solved by the backward substitution as in [2].

FIG. 4.5-4.6 show the density profiles at different times computed by the standard filtered Fourier spectral simulation. As shown in ([15], [17]), the sharp front density is developed from a smooth initial profile in the later time. Due to nature of the computational method, the non-physical oscillations start to appear when the numerical solution reaches to the situation having almost singularity in time if the numerical solution is under-resolved. The one dimensional cuts of the density at $y = \pi$ at different times are shown in FIG. 4.7. Due to the overshoot and undershoot of the Gibbs, the minimum(=0.0) and the maximum(=5.3084) value of the density are poorly represented in FIG. 4.7.

One can effectively recover non-oscillatory solution by mitigating the Gibbs oscillations in use of the Fourier-Padé reconstruction as a postprocessing to the numerical solutions by the filtered Fourier collocation method.

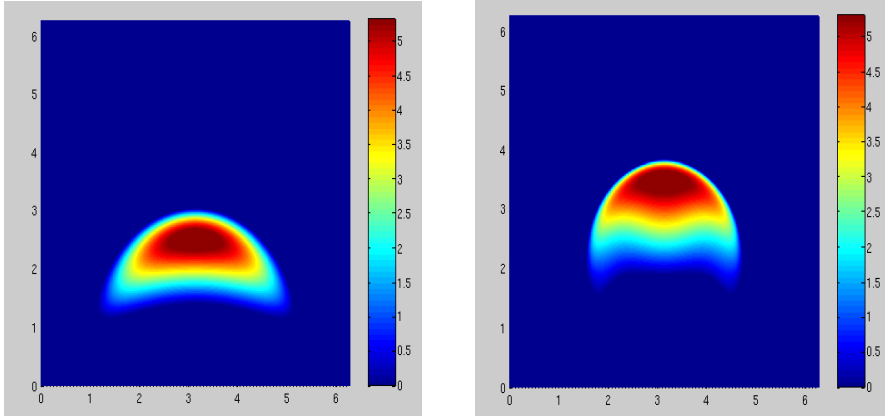


FIG. 4.5. The density contour of the Boussinesq equations at $t = 0.0$ (Left) and $t = 1.1$ (Right) by the Fourier collocation methods on grids 512^2 .

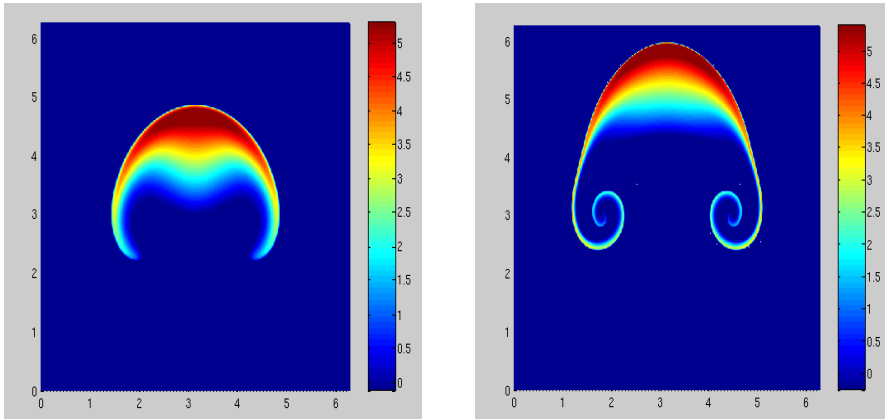


FIG. 4.6. The density contour of the Boussinesq equations at $t = 2.2$ (Left) and $t = 3.0$ (Right) by the Fourier collocation methods on grids 512^2 .

For the Fourier-Padé reconstruction procedure, the Fourier modes from the top spectrum are discarded same as done for the Burgers' equation due to the fact that the lower spectrum of the Fourier modes are accurately resolved and the numerical errors are usually associated with the high modes. Thus in order to get the best reconstruction one has to take the cut-off frequency N_c reasonably.

In FIG. 4.7-4.12, the numerical results show the time history of the minimum and maximum values of the density before and after the Fourier-Padé reconstruction procedure. One can observe that, for all practical purposes, the Gibbs overshoot and undershoot are effectively removed even for the cases of the small scale structure shown in FIG. 4.11 and FIG. 4.12.

5. Conclusion. Using the idea of rational approximation based on Fourier series, we have defined the explicit representations of the Fourier-Padé-Galerkin approximation and the Fourier-Padé collocation approximation in terms of the given continuous and discrete Fourier coefficients, respectively.

The numerical results for the Fourier-Padé-Galerkin and Fourier-Padé collocation

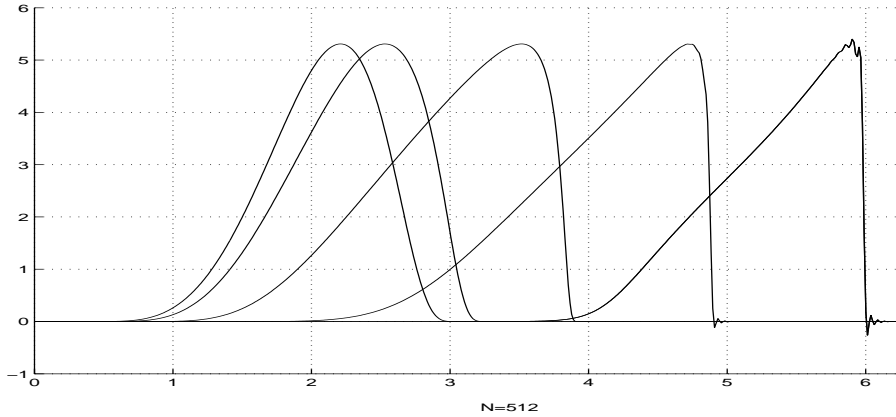


FIG. 4.7. Evolution of density along the symmetry axis $x = \pi$ by the filtered (order=16) Fourier method on grids 512^2 .

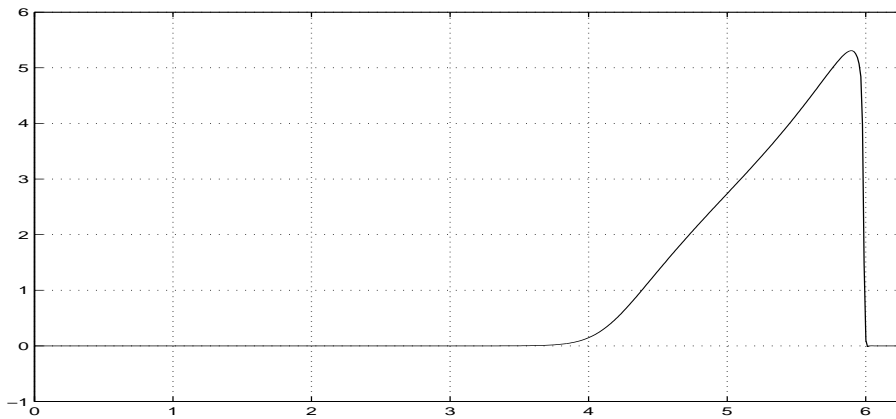


FIG. 4.8. Density along the symmetry axis $x = \pi$ after the reconstruction by Fourier-Padé collocation method on grids 512^2 , $N_c = 137$, $M = 46$.

methods are provided, which show the successful mitigation of the Gibbs oscillations away from the singularity with spectral convergence as the grids are refined and the degree of the denominator is increased.

The numerical simulations for the inviscid Burgers' equation and two dimensional incompressible Boussinesq convection flow show the successful reduction of the Gibbs oscillations in the standard Fourier spectral simulations after a post-processing by the Fourier-Padé reconstruction.

Acknowledgments. The authors thank David Gottlieb for the support of this project and suggestion of useful ideas. The conversation with Jan S. Hesthaven and Laura Lurati has been helpful.

References

- [1] G. K. BATCHELOR, *The stability of a large gas bubble moving through a liquid*, J. Fluid Mech. 184, 399(1987).

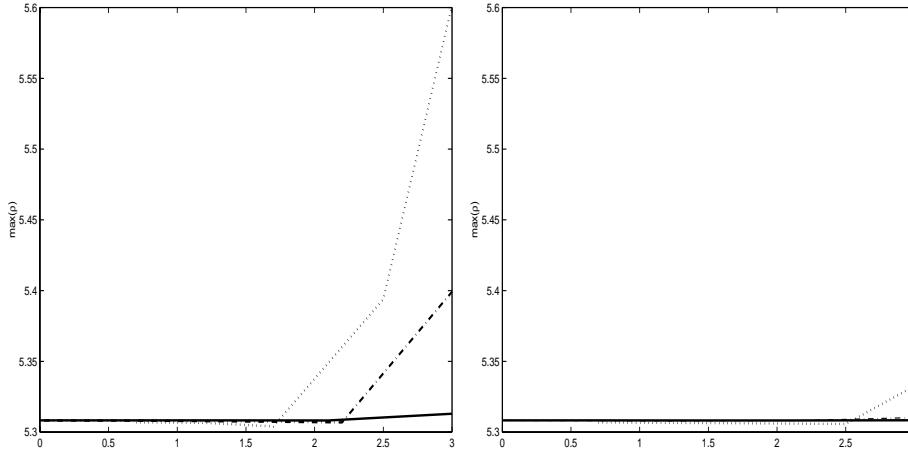


FIG. 4.9. Time history of the maximum density along the symmetry axis $y = \pi$: filtered Fourier(left) and after the Fourier-Padé reconstructions(right) with dots on grids 256^2 , $M = 64$, $N_c = 14$, dash-dot on grids 512^2 , $M = 24$, $N_c = 24$, solid line on grids 1024^2 , $M = 34$, $N_c = 34$.

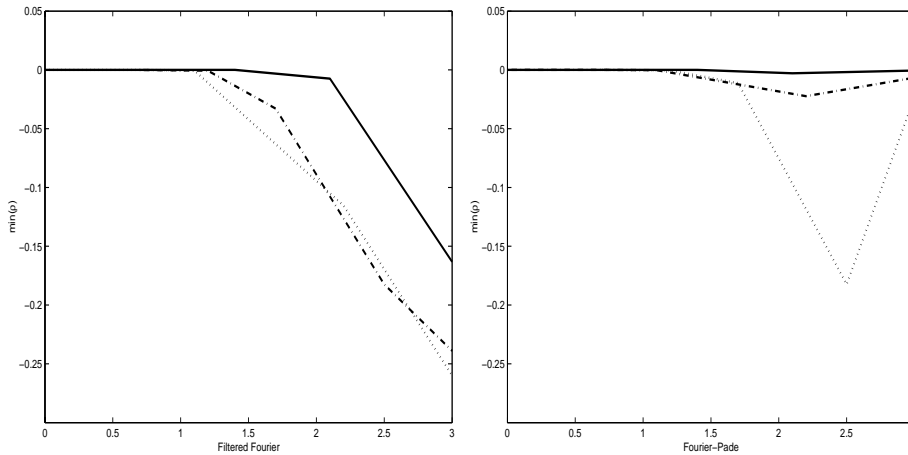


FIG. 4.10. Time history of the minimum density along the symmetry axis $y = \pi$: filtered Fourier(left) and after the Fourier-Padé reconstructions(right) with dots on grids 256^2 , $M = 64$, $N_c = 14$, dash-dot on grids 512^2 , $M = 24$, $N_c = 24$, solid line on grids 1024^2 , $M = 34$, $N_c = 34$.

- [2] R.H. BARTELS, G.W. STEWART, *Algorithm 432, solution of the matrix equation $Ax + xB = C$* , Comm. ACM 15 (1972), pp. 820-826.
- [3] J. T. BEALE, T. KATO, A. MAJDA, *Remarks on the breakdown of smooth solutions for the 3-D Euler equations*, Comm. Math Phys 94, 61(1984).
- [4] H. CABANNES, *Padé approximants method and its applications to mechanics*, Lecture notes in physics edited by J. Ehlers, K. Hepp, H. A. Weidenmüller, J. Zittartz, Springer-Verlag, New York, 1976.
- [5] A. DOLD, B. ECKMANN, *Padé approximation and its application*, Springer-Verlag, Berlin Heidelberg, New York, 1979.
- [6] L. EMMEL, S.M. KABER AND Y. MADAY *Padé-Jacobi filtering for spectral approximations of discontinuous solutions* accepted for publication in Numerical Algorithms, 2002.

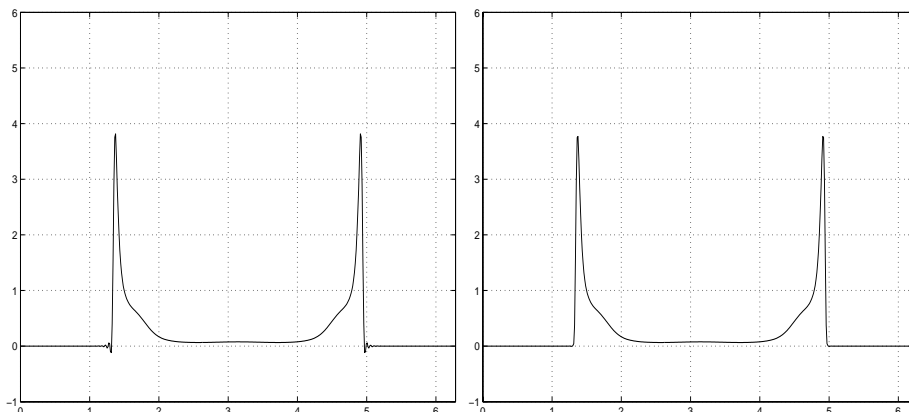


FIG. 4.11. The density along the symmetry axis $y = 3.91$ at $t = 3.0$ by filtered Fourier collocation method(left) and after the Fourier-Padé reconstruction(right) on grids 512^2 , $M = 26$ and $N_c = 136$

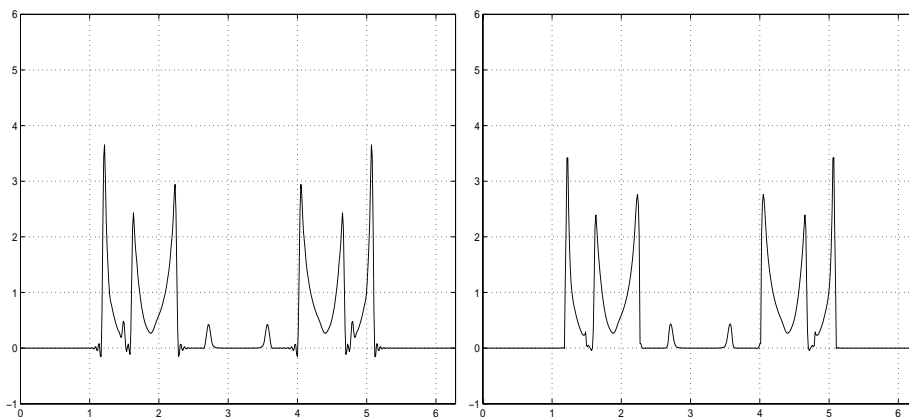


FIG. 4.12. The density along the symmetry axis $x = \pi$ at $t = 3.0$ by filtered Fourier collocation method(left) and after the Fourier-Padé reconstruction(right) on grids 512^2 , $M = 49$ and $N_c = 148$

- [7] T. A. DRISCOLL, B. FORNBERG *Padé algorithm for the Gibbs phenomenon*, submitted for publication in Numerical Algorithms, 2000.
- [8] J.F. GEER *Rational trigonometric approximations using Fourier series partial sums*, Journal of Sci. Comp., **10** (1995), n. 3.
- [9] J. GIBBS, *Fourier's series*, letter in Nature, 59, pp.200, 1898.
- [10] D. GOTTLIEB, M. Y. HUSSAINI AND S. A. ORSZAG, *Introduction: Theory and Applications of Spectral Methods*, in Spectral Methods for Partial Differential Equations, R. Voigt, D. Gottlieb and M.Y. Hussaini, ed. SIAM, Philadelphia, 1984. pp. 1-54.
- [11] D. GOTTLIEB, S. A. ORSZAG, *Numerical Analysis of Spectral Methods : Theory and Application*, CMBS-NSF Regional Conference Series in Applied Mathematics 26, SIAM, Philadelphia, 1977.
- [12] D. GOTTLIEB, C. W. SHU, *The Gibbs phenomenon and its resolution*, SIAM review, 39, pp.644-668, 1997.

- [13] H. PADÉ, *Mémoire sur les développements en fractions continues de la fonction exponentielle pouvant servir d'introduction à la théorie des fractions continues algébriques*, Ann. Fac. Sci. de l'Ec. Norm. Sup., 16, pp.395-436, 1899.
- [14] A. PUMIR, E. D. SIGGIA, *Development of singular solutions to the asyymmetric Euler equations*, Phys. Fluids A 4, 1472(1992).
- [15] WEINAN E, C.W. SHU, *Small-scale structures in Boussinesq convection* , Phys. Fluids 6(1), 1994.
- [16] E.B. SAFF, R.S. VARGRA, *Pade and rational approximation: Theory and application*, Academic press, Inc., New York, 1977.
- [17] TAO TANG, ZHENGRU ZHANG, *Resolving small-scale structures in Boussinesq convection by adaptive grid methods*, 2003(preprint).
- [18] H. VANDEVEN, *Family of spectral filters for discontinuous problems*, J. Sci. Compt. 6, 159(1991).